Minimally Invasive Online Water Monitor

A. S. Holmes, *Member, IEEE*, M. E. Kiziroglou, *Senior Member, IEEE*, S. K. E. Yang, C. Yuan, D. E. Boyle, *Member, IEEE*, D. M. Lincoln, J. D. J. McCabe, P. Szasz, S. C. Keeping, D. R. Williams, and E. M. Yeatman, *Fellow, IEEE*

***Abstract*—Sensor installation on water infrastructure is challenging due to requirements for service interruption, specialized personnel, regulations and reliability as well as the resultant high costs. Here, a minimally invasive installation method is introduced based on hot-tapping and immersion of a sensor probe. A modular architecture is developed that enables the use of interchangeable multisensor probes, nonspecialist installation and servicing, low-power operation and configurable sensing and connectivity. A prototype implementation with a temperature, pressure, conductivity and flow multisensor probe is presented and tested on an evaluation rig. This article demonstrates simple installation, reliable and accurate sensing capability as well as remote data acquisition. The demonstrated minimally invasive multisensor probes provide an opportunity for the deployment of water quality sensors that typically require immersion, such as pH and spectroscopic composition analysis. This design allows dynamic deployment on existing water infrastructure with expandable sensing capability and minimal interruption, which can be key to addressing important sensing parameters, such as optimal sensor network density and topology.**

***Index Terms*—Hot-tapping, installation, multisensor, quality, sensor, water.**

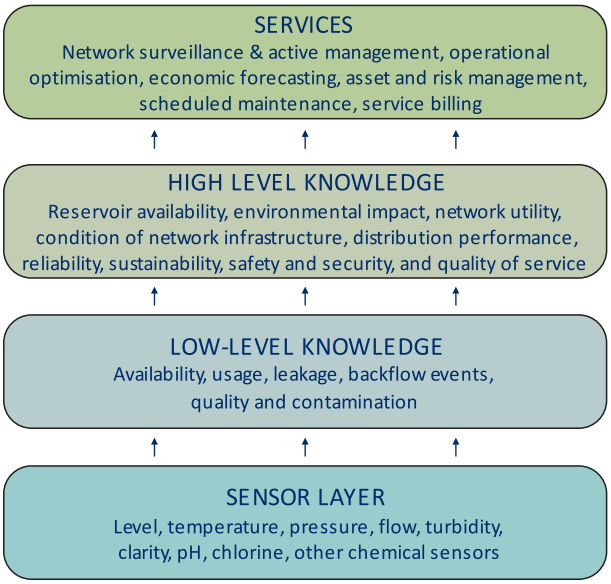

Fig. 1. From sensor to service: a hierarchical overview of water sensing technology.

I. Introduction

THE OBJECTIVE of monitoring water infrastructure is to facilitate a safe, sustainable, reliable and cost-effective service. Water distribution wireless sensor networks typically employ sensors measuring various quantities, including level, temperature, pressure, flow, turbidity, pH, chlorine concentration, as well as other chemical properties [1]–[3]. They provide low-level knowledge, such as availability, usage, leakage, backflow events, quality, and contamination. This information can be transformed into higher level knowledge, such as reservoir availability, environmental impact, network utility, condition of network infrastructure, distribution performance, reliability, sustainability, safety and security, and quality of service. Such system knowledge can underpin services, including network surveillance and active management, operational optimization, economic forecasting, asset and risk management, scheduled maintenance, and service billing, and may be extended to irrigation scheduling in precision agriculture and management of decentralized systems like gray water reuse networks [4]. A schematic overview of this hierarchy for water sensing technology is shown in Fig. 1.

Wireless sensing technologies have been rapidly advancing in the last decade, offering multiple sensors, powerful data processing and fast remote communication capabilities to water networks. In addition, abstractive data analysis software enables new opportunities for node and network level intelligence. At a sensor node level, various integrated water quality systems have emerged recently. For example, in [5], a single-substrate pH, chlorine and temperature electrochemical multisensor is demonstrated as an *in-situ* analysis system, in integration with a commercial microcontroller and communication platform or a field programmable gate array (FPGA) microchip [6]. An ultraviolet–visible spectrophotometry analyzer has also been developed for chemical oxygen demand and ammonia-nitrogen determinations [7].

Manuscript received 1 December 2020; revised 16 March 2021 and 3 April 2021; accepted 9 April 2021. Date of publication 19 April 2021; date of current version 8 August 2022. This work was supported by ABB Switzerland Ltd, Group Technology Management. *(Corresponding author: M. E. Kiziroglou.)*

A. S. Holmes, S. K. E. Yang, and E. M. Yeatman are with the Department of Electrical and Electronic Engineering, Imperial College London, London SW7 2AZ, U.K.

M. E. Kiziroglou is with the Department of Electrical and Electronic Engineering, Imperial College London, London SW7 2AZ, U.K., and also with the Department of Industrial Engineering and Management, International Hellenic University, 570 01 Thermi, Greece (e-mail: m.kiziroglou@imperial.ac.uk).

C. Yuan and D. R. Williams are with the Department of Chemical Engineering, Imperial College London, London SW7 2AZ, U.K.

D. E. Boyle is with the Dyson School of Design Engineering, Imperial College London, London SW7 2AZ, U.K.

D. M. Lincoln, J. D. J. McCabe, P. Szasz, and S. C. Keeping are with ABB, St. Neots PE19 8EU, U.K. (e-mail: david.lincoln@gb.abb.com).

Digital Object Identifier 10.1109/JIOT.2021.3074081

Unresolved challenges in the state-of-the-art solutions of this type include efficient energy provision and management at the sensor node level, and installation requirements which are often not compatible with existing water distribution infrastructure. This challenge is especially important because existing, predominantly old infrastructure is more prone to leakage, quality issues and malfunction and is therefore a priority for monitoring. Typically, commercial water monitoring systems require the insertion of a separate pipe assembly containing the measurement devices into the pipeline [8]–[10]. This necessitates major interruptive installation works, involving valve-to-valve underground access, specialized personnel, and the installation of pipe assemblies with different materials and technologies. These are key limiting factors for the large-scale deployment of sensor networks in water infrastructure. Noninvasive, acoustic technologies for pipeline corrosion monitoring have been used successfully, mainly as portable diagnostic tools, and such methods for sensing other quantities, including liquid flow, have been commercialized in recent years [11], [12]. However, these acoustic methods still face a number of challenges around their installation and operation. On the other hand, water quality metrics, such as pH, conductivity, and spectroscopic analysis require direct contact with the water sample of interest.

In this article, a minimally invasive method for installing sensor nodes on existing water distribution infrastructure is presented. It is based on a small-scale hot-tapping method and the insertion of a small diameter sensing probe with a multisensing head. A prototype system has been developed, including a tapping and sealing mechanical design adaptable to pipe diameters in the 25–300-mm range with interchangeable multisensor probes, integrated with data acquisition, processing, transmission and cloud reception capabilities. Device tests demonstrate successful installation and acquisition of calibrated data with adequate accuracy for water temperature, flow, pressure and conductivity, as well as for external temperature, pressure and vibration sensing. Some of the ideas and findings reported in this article are being protected.

This article is organized as follows. The minimally invasive hot-tapping method is introduced in Section II. The design and fabrication of the mechanical and electronic components of the prototype sensor system are presented in Sections III and IV, respectively. A water flow test rig developed and used as an evaluation setup is presented in Section V. In Section VI, experimental sensor test results are presented and discussed. This article concludes in Sections VII and VIII by discussing the benefits and opportunities arising from minimally invasive multisensors for water networks.

II. Minimally Invasive Multisensor

A. Sensor Overview

Our aim in this work was to demonstrate a compact and rapidly deployable multiparameter wireless sensor node that could monitor at least three of the following quantities at a single location within the water distribution network: pressure, temperature, flow, conductivity, pH and turbidity. The inclusion of conductivity, pH and turbidity in this list precluded an entirely noninvasive approach, and consequently the device reported here is invasive, requiring a small access hole in the pipe wall. However, by exploiting state-of-the-art sensor technology we have been able to limit the diameter of this access hole to just 6.3 mm. At this size the hole has negligible effect on the mechanical integrity of the pipe, and as such we describe the sensor as *minimally invasive*.

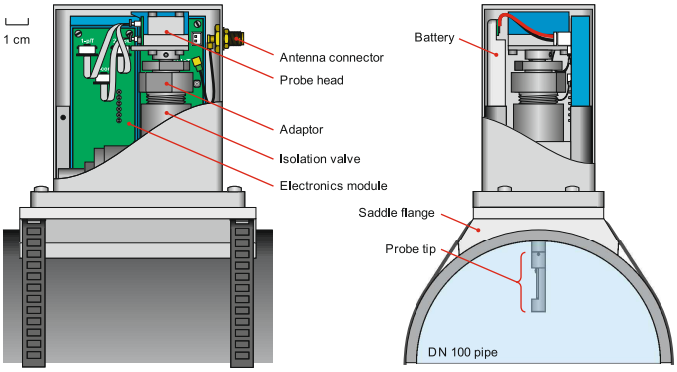

Fig. 2. Minimally invasive sensor node comprising saddle flange, sensor port (isolation valve on baseplate), probe adaptor, sensor probe, electronics module, and battery.

Fig. 2 shows a sketch of a prototype sensor node mounted on a DN 100 (114.8-mm diameter) pipe. At the core of the device is a 6.0-mm diameter sensor probe which protrudes into the flow and carries the sensing elements, in this case a combined pressure/temperature sensor, a conductivity sensor and a differential pressure sensor which is used to measure the flow speed. The probe passes through an isolation valve which allows the access hole to be closed off during installation and replacement of the probe. A commercial ball valve has been used in the prototype; however, in future we expect to replace this by a customized gate valve as this will allow a reduction in the overall size of the sensor node. The isolation valve is mounted on a baseplate which interfaces to the pipe via a saddle flange. The isolation valve and baseplate together are referred to as the *sensor port*.

The sensor outputs are fed to an electronics module which consists of a sensor-specific *frontend* submodule and a generic *main* submodule. The frontend submodule contains the sensor readout circuits and a low-power microcontroller unit (MCU) for managing the sensors and digitizing the sensor readings. The main submodule contains a wireless MCU with Bluetooth capability, a narrowband IoT (NB-IoT) MCU, an secure digital (SD) card for data logging and additional environmental sensors for temperature, humidity and acceleration/vibration. Communication between the submodules is via a 2-wire serial link. Power for the sensors and electronics is provided by a 4800-mAh lithium-polymer battery.

The sensor node is enclosed in a stainless-steel housing which is sealed to IP68. An SMA connector in the housing wall allows a whip antenna to be mounted directly on the device; alternatively, a cable can be run to a remote antenna, for example when the sensor node is deployed underground. The housing is 75-mm long (axial direction) and 50-mm wide, and the height from the bottom of the baseplate is 95 mm. The

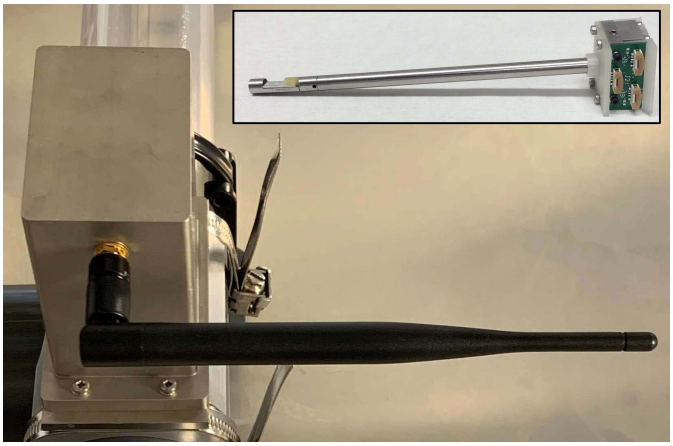

Fig. 3. Picture of the complete enclosed system as installed on a water flow test rig. A picture of the multisensor probe is shown in the inset.

complete sensor node installed on a sensor test rig is shown in Fig. 3. The multisensor probe is shown in the inset.

B. Sensor Installation

A key requirement for the minimally invasive sensor node was that it should be possible to install the device by hot tapping, i.e., without interrupting the flow of water in the pipe. A custom hot-tapping tool was designed for this purpose. This Section outlines the hot-tapping procedure which takes around 30 min for a metal-walled pipe.

The first step is to mount the saddle flange, securing it to the pipe with steel straps and/or adhesive. A water-tight seal is formed between the flange and the pipe wall either by an O-ring or a gasket. The sensor port is then mounted on the saddle flange, and hot-tapping is carried out as outlined in Fig. 4. The hot-tapping tool consists essentially of a drive shaft that sits between a standard electric drill and the drill bit. The drive shaft moves inside a cylinder which acts as a drill guide and also forms a seal that prevents escape of the water that leaks from the pipe once the pipe wall has been breached. The drive shaft is hollow, allowing cutting fluid to be fed to the drilling zone if a suitable "oil-feed" drill bit with coolant channels is deployed.

The hot-tapping tool is screwed into the valve port, and the valve is opened to allow access to the pipe wall. Drilling then proceeds with a suitable water-based cutting fluid being applied through the drill bit. As in any machining operation, the cutting fluid provides cooling and lubrication, and also carries swarf away from the drilling zone. The cutting fluid is replaced by water before the pipe wall is breached, and once drilling is complete the water leaking from the pipe is used to flush the valve [Fig. 4(b)]. To complete the process the drill is withdrawn, the valve is closed [Fig. 4(c)] and the tool is removed from the valve port [Fig. 4(d)].

To complete the sensor node installation, the sensor probe is inserted (see Section III), the electronics module and battery are fitted, and a basic functional test is carried out. Finally, the housing is screwed into place. These steps take approximately 10 min, so the overall installation time for the sensor node, including hot-tapping, is around 40 min.

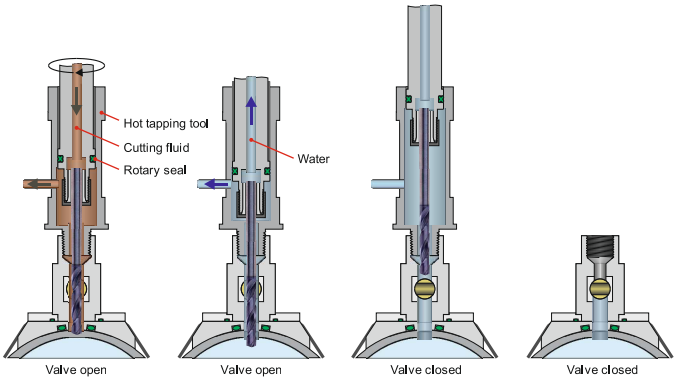

Fig. 4. Hot tapping procedure showing: (a) initial drilling phase with through-tool delivery of cutting fluid; (b) end of second drilling phase, with flushing of valve bore by process water; (c) after withdrawal of cutter and closure of isolation valve; and (d) after removal of hot-tapping tool.

TABLE I
SENSOR CHIPS IN PROTOTYPE PROBE

Measurand	Part number	Specified range
Pressure	H1T-0170-L2T	0 to 10 bar absolute
Temperature	H1T-0170-L2T	–40 to +150 °C (p-n diode)
Flow (by delta-p)	AMS 5195-0200-D-B	–200 to +200 mbar
Conductivity	LFS1305	0.1 to 200 mS/cm

III. MULTISENSOR PROBE DESIGN

A. Probe Structure

Table I shows the sensor elements included in the prototype multisensor probe reported here. The static water pressure is monitored by a silicon absolute pressure sensor with piezoresistive readout (Merit Sensor type H1T-0170-L2 [13]). This device also incorporates a p-n diode for temperature compensation, which is also used to monitor the water temperature. The sensor is $2.1 \times 2.1 \times 1.4$ mm^3 in bare die format, making it small enough to be accommodated in the end of the 6 mm-diameter probe tip.

The local flow velocity is measured using the differential pressure technique [14]. Here, the flow speed is inferred from the pressure difference that naturally arises between points fore and aft on a bluff body (in this case the probe tube) placed in the flow. This approach is well known in larger scale systems and in this work we have adapted it and demonstrated its efficacy at small scale.

As it was not possible to source a differential pressure sensor small enough to fit within the probe tube, the sensor chip (Analog Microelectronics GmbH type AMS 5195-0200-D-B, [15]) is housed in the probe head, and the fore and aft pressures at the probe tip are conveyed to the chip via 1.0 mm internal diameter stainless-steel capillaries. Currently these capillaries are open and filled with air when the probe is installed.

The fourth sensor in the prototype probe is a conductivity sensor (Innovative Sensor Technology AG type LFS1305, [16]) comprising an array of parallel electrodes on

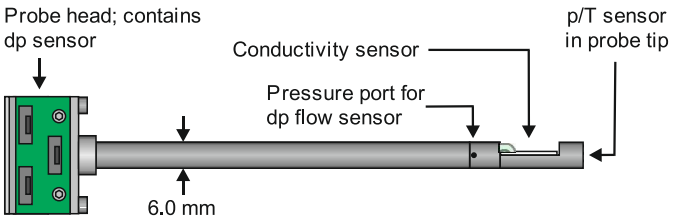

Fig. 5. Minimally invasive sensor probe incorporating pressure, temperature, flow, and conductivity sensors.

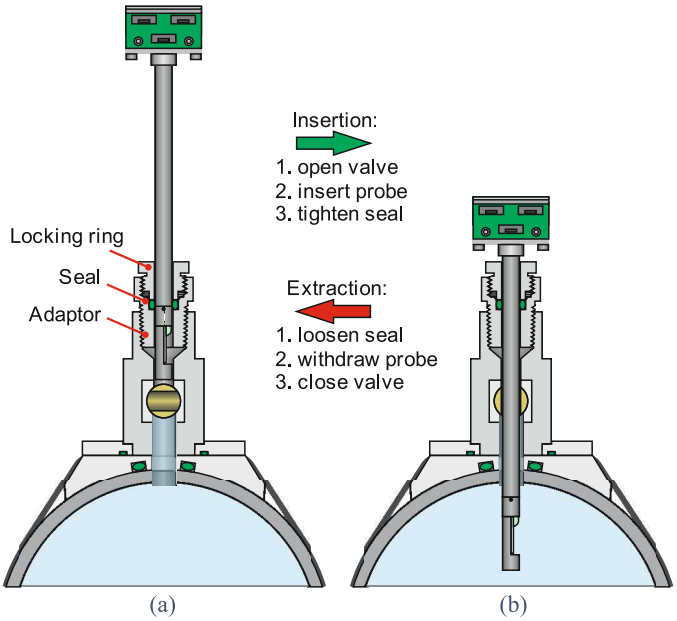

Fig. 6. Procedures for "hot" insertion (a)→(b) and extraction (b)→(a) of minimally invasive sensor probe.

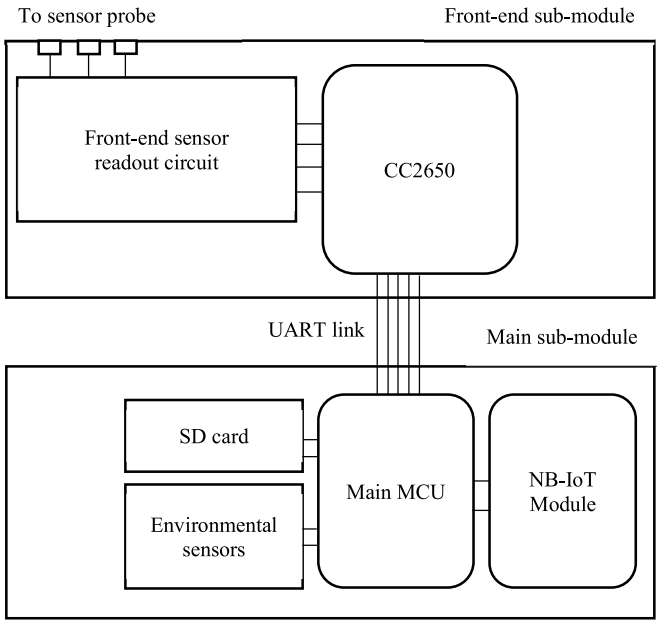

Fig. 7. System diagram of the sensor node electronics, with frontend submodule and main submodule as indicated.

TABLE II
ENVIRONMENTAL SENSOR CHIPS

Measurand	Sensor type	Specified range
Humidity	Si7021-A20	0-80% RH
Temperature	Si7021-A20	−10 to 85 °C
Acceleration	LIS3DH	Dynamically selectable ±2g/±4g/±8g/±16g

a ceramic substrate, accommodated as shown in Fig. 5. This device works by making a 4-point measurement where the outer electrodes are driven with an AC excitation voltage and the conductivity is estimated from the ratio of the excitation current to the voltage measured between the inner electrodes.

Fig. 5 shows the overall layout of the prototype multisensor probe and a cut-away detail of the probe tip showing how the p/T and conductivity sensors are positioned and how their electrical connections are routed to the probe head. The components in the probe tip are potted in a water-resistant epoxy that is expected to allow continuous submersion in cold water for several years.

B. Probe Installation and Replacement

The inclusion of an isolation valve on the sensor port makes it possible to "hot-swap" the multisensor probe, i.e., replace it without interrupting the flow in the pipe. Fig. 6 outlines the procedures for inserting and removing the probe. Before installing the probe, a probe adaptor is screwed into the valve port. This part incorporates a seal that can be tightened down onto the probe tube by means of a locking ring.

To insert a new probe, the probe is inserted into the adaptor so that it stops just short of the isolation valve, as shown in Fig. 6(a). The valve is then opened and the probe is inserted into the flow. Finally the locking ring is tightened to improve the integrity of the seal [Fig. 6(b)]. To remove the probe the above sequence is simply reversed: the seal is loosened, the probe is partially withdrawn, and the valve is closed. The probe can then be completely withdrawn without any water escaping. The entire hot-swapping process, including disconnection and reconnection of the probes, can be completed in several minutes. Ease of replacement is an important consideration for probes incorporating chemical sensors as these generally have lifetimes measured in months rather than years.

IV. SENSOR NODE ELECTRONICS

A. Sensor Node Electronics

Fig. 7 shows the system diagram of the sensor node electronics being divided into two submodules. The frontend module consists of readout circuits that connects to the sensor chips in the prototype probe via flexible flat cables (FFCs) and flexible printed circuit (FPC) connectors. The Texas Instruments CC2650 chip is a low-power MCU employed to support the readout circuit for the prototype sensor probe.

A DC/DC converter is used to provide 5 V for the pressure and conductivity sensors [17]. The outputs of the pressure sensor and the temperature diode are amplified using instrumentation amplifiers to take advantage of the full scale of the MCU's ADC channels. The differential pressure sensor only

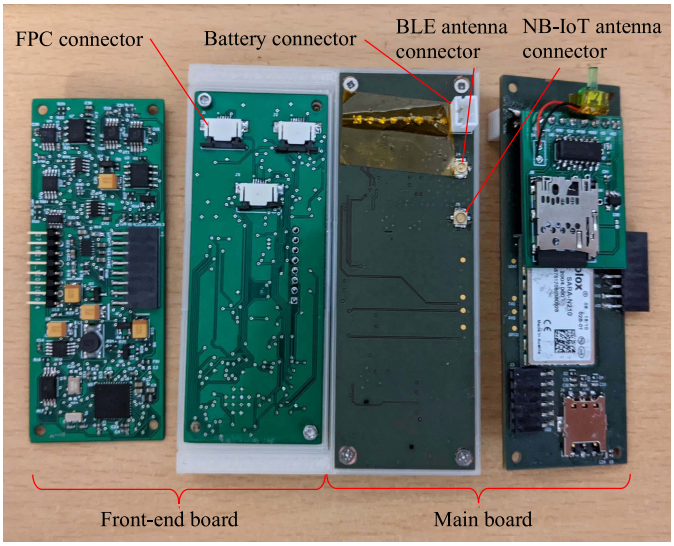

Fig. 8. Frontend and main circuit boards. From left to right: Back view of the frontend board, front view of the frontend board (in compartment), front view of main board (in compartment), and back view of main board.

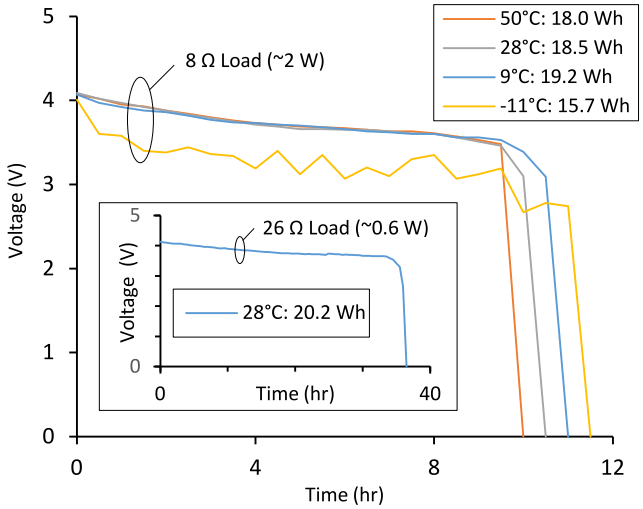

Fig. 9. LP735977JH battery discharge test at different temperatures.

requires 3.3 V as power supply so it can be powered up by the GPIO pins of the MCU, and its data is obtained using I^2C.

The conductivity sensor requires an AC excitation signal to prevent electrolysis so that the concentration of ions in the solution remains constant. Therefore, a switching regulator is used to produce ±5 V supply rails and using PWM from the MCU, an AC voltage signal of 5 kHz is produced for the sensor. The AC signal is fed into an amplifying drive circuit comprising an inverting amplifier with switchable gain so that the sensor gives two measurement ranges—0–100 μS/cm and 0–10 mS/cm. The resulting signal is then converted back to DC and read by an ADC channel of the MCU.

Once the frontend sensor data is obtained, it is compiled and sent to the main submodule via UART. The main MCU in the module is the nRF52840, a multiprotocol System on Chip (SoC) with Bluetooth low energy (BLE) capability [18]. It offers low energy consumption through an adaptive power management system, and library support for external SD storage through a serial peripheral interface (SPI), which is important for local data storage during offline operation. The nRF52840 communicates with a second MCU, the SARA-N2 [19] power-optimized NB-IoT module, to provide cellular connectivity and large geographic area coverage. Additional environmental sensors (Si7021-A20 [20] and LIS3DH [21]) are also connected to the nRF52840 using I^2C. The environmental sensor details are shown in Table II.

Fig. 8 shows a photograph of the frontend submodule (left) and the main submodule (right). The main submodule has two boards stacked together for confinement within the sensor port housing. The smaller board contains the SD card circuit and power-on indicator LED whereas the rest of the circuits are implemented on the larger board.

B. Connectivity/Acquisition

The system comprises three communication interfaces. The first interface is a local USB interface. It offers initial programming, testing and servicing through the Joint Test Action Group (JTAG) interfaces of the MCUs and their respective development boards, using a computer and a simple network terminal interface, such as PuTTY [22]. This interface also makes the electronic architecture expandable to provide local display and external digital connectivity during normal operation.

Further to the local communication interface available for both submodules, the main board provides a BLE and an NB-IoT interface for local and cellular data transfer. The nRF52840 uses Bluetooth 5 Low Energy, which allows communications at distances over 240 m, which is about 4 times the range of Bluetooth 4.2 and has a higher bit rate of 2 Mb/s [23]. The nRF52840 also communicates with the SARA-N2 to establish Internet connection using NB-IoT. NB-IoT is a standards-based low-power wide area network (LPWAN) technology that has low-power consumption and wide area coverage [24]. It uses a narrower bandwidth compared to LTE-M which allows for better indoor/underground penetration [24]. An survey of IoT and upcoming 5G connectivity solutions can be found in [25].

C. Power Supply and Energy Management

The battery used for the prototype is the 3.7 V, 4800 mAh lithium polymer LP735977JH by Jauch Quartz GmbH [26]. A discharge test was done to verify the performance of the battery at different temperatures, using a 2 W (8Ω) load, which is 67% of the 0.2°C (3 W) load at which the nominal capacity is specified. The resulting discharge curves and battery capacities calculated by discrete integration are shown in Fig. 9. The battery cuts off at around 10–11 h, demonstrating adequate operation as expected by nominal specifications, for all temperatures. In the −11°C test, a varying voltage drop is observed, which is attributed to a reduction of Li ion mobility in the polymer electrolyte.

An additional test at a lower, 0.6 W (26Ω) load was performed, which corresponds to the expected maximum

TABLE III
NOMINAL CURRENT CONSUMPTION OF DIFFERENT COMPONENTS AND PERIPHERALS

Components (including readout circuit)	Required peripherals/Protocols	Current consumption
Pressure sensor	-	10 mA
Differential pressure sensor	-	2.5 mA
Conductivity sensor	PWM by CC2650	47-62 mA
Humidity & temperature sensor	Standby mode	0.06 μA
	Power up / I2C operation	3.5 mA
Accelerometer	1 Hz sample rate	2 μA
CC2650	Sleep mode	1.2 μA
	ADC + I2C + UART (Sensor controller task running at 1 Hz)	7.5 μA
nRF52840	Sleep mode	2 uA
	UART / I2C	0.6 mA
	Advertising (1s interval)	10 μA
	Connected (75ms interval)	1 mA
SARA-N2	Sleep mode	3 μA
	3 dBm Tx power	78 mA

TABLE IV
CURRENT CONSUMPTION TABLE FOR FRONTEND AND MAIN BOARDS. AVERAGE SUPPLY VOLTAGE = 3.6 V

Components \ Configuration		1: Frontend sensors + environmental sensors + BLE	2: Frontend sensors + environmental sensors + NB-IoT
Front-end sensor samples per minute	Conductivity	15	15
	p/T	5	5
	DP	5	5
Env. Sensors samples per minute		60	60
Front-end sensors ON time (s)		2	2
Env. Sensors ON time (s)		0.06	0.06
nRF52840 UART ON time (s)		15	15
BLE data transmission time (s)		10	-
NB-IoT data transmission time (s)		-	180
Average consumption (mA)		0.34	0.5

system power consumption. The results, shown in the inset of Fig. 9 demonstrated a capacity of 20.2 Wh, which is again within the nominal battery specification tolerance range.

The duration of power autonomy offered by the battery depends on system usage. For example, if it is assumed that the battery should power the device for at least a year, the average current consumption should be lower than 0.55 mA. The MCUs provide various sleep and low-power operation modes which can be employed by duty cycling in accordance with a given sensing scenario, to obtain the desired balance between power autonomy duration and average current consumption, i.e., sensing intensity.

Table III shows the nominal current consumption for each system component. Significant current is consumed by the conductivity sensor circuit and during SARA-N2 transmission, which is set at −3 dBm. It is apparent that continuous high sampling rates would result in unacceptably high power consumption. Therefore, different sensors and their required MCU peripherals need to be duty cycled. For example, sampling the conductivity sensors for 2 s every 15 min and the other sensors for 2 s every 5 min yields an average current consumption below 0.3 mA.

Duty cycling can also be used in operating the internal and wireless communication modules of the system. The main-submodule has the option to either use BLE or NB-IoT depending on the application. The nRF52840 uses a UART to receive data from the frontend module To prevent it from consuming a constant 0.6 mA as shown in Table III, the UART can be turned on only for a brief period of time, e.g., for 15 s when the frontend board is ready to send data. Wireless data transmission can be performed at a very low duty cycle (e.g., 0.2% or 180 s per day) to reduce the power used by BLE or NB-IoT. Sensor data is stored locally in an external SD card before the bulk of data is transmitted.

An example duty cycling operation scenario that allows a 1-year power autonomy with the selected battery is summarized in Table IV, for the cases of BLE and NB-IoT. The data transmission time accounted for NB-IoT is significantly longer as it requires time to connect to a supported base station and establish an Internet connection, but it may still allow several communication sessions within a 24-h period.

Adding both current consumption for the frontend submodule and main submodule gives a resultant current consumption of 0.34 mA (BLE) and 0.5 mA (NB-IoT) as shown in Table IV. More changes can be made to reduce the current consumption further, for example by reducing the sampling rate of the environmental sensors, increasing the advertising and connection interval for BLE, or reducing the transmission power of the BLE/NB-IoT signal.

V. EVALUATION SETUP

To examine the performance of the prototype, we built a flow rig and a static pressure test rig to conduct experimental evaluation tests. ISO 5167 [27] states that a specific minimum length of upstream and downstream pipe should be installed before and after pressure differential devices. Considering the availability and dimension of the test facility, a flow rig with 1-inch and 2-inch test sections was built, which is shown in Fig. 10. Water is pumped from the water tank using the CRESTPUMP AM-50 water pump into the test sections controlled by a Parker AC10 motor controller. An ABB FEP611 electromagnetic flow meter was used as the reference volumetric flow meter with an accuracy of 0.4%.

The water distribution system commonly uses 4-inch and 6-inch pipes , therefore we built another 4-inch static pressure test rig, which is displayed in Fig. 11, to evaluate the sealing and the pressure sensor. The reference value of pressure was given by WIKA DG-10 pressure gauge with an accuracy of 0.5%, and a pressure relief valve was installed for protection

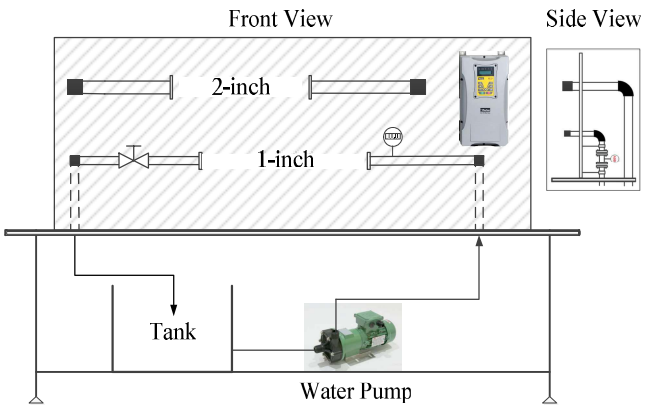

Fig. 10. Water flow test rig layout.

Fig. 11. Static pressure test rig.

in case of excess pressure. The pressure range of the static test rig was 0-10 bar.

VI. System Characterization

The test rigs described above were used to evaluate the performance of the pressure, temperature, conductivity and flow sensors in the prototype multisensor node.

Pressure sensor testing was carried out on the static test rig of Fig. 11. In total 5 runs were launched in the range of 0 to 8 bar. The results are shown in Fig. 12. A correlation between sensor output and reference pressure value was established according to the data of 4 runs

$$P = 4.2103 \cdot V_p - 1.0863 \tag{1}$$

where P denotes gauge pressure (bar) and V_p denotes voltage output (V) of the pressure sensor. The fifth test run as shown in the inset of Fig. 12 was used to evaluate (1) and the relative errors ranged from -0.69% to 0.19%.

The temperature sensor was tested in a Spark Holland Mistral temperature control device. The temperature accuracy and stability of this device were found to be better than 0.1°C. The reference temperature meter was Rotronic HP32/HC2, which has a nominal 0.1°C accuracy itself. The temperature

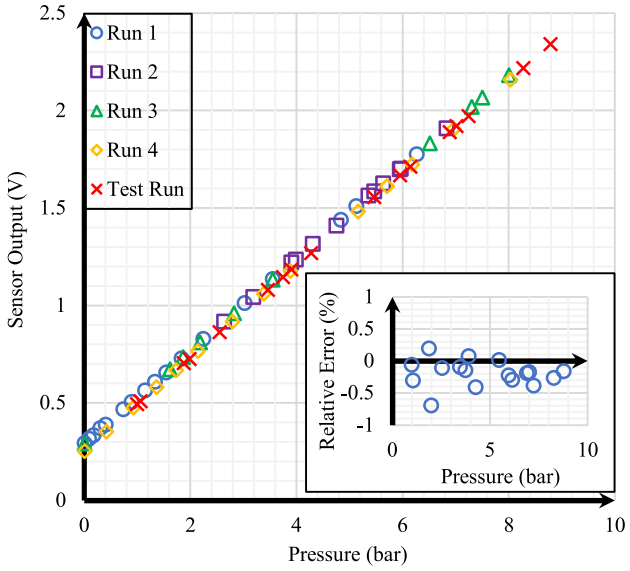

Fig. 12. Performance of the pressure sensor.

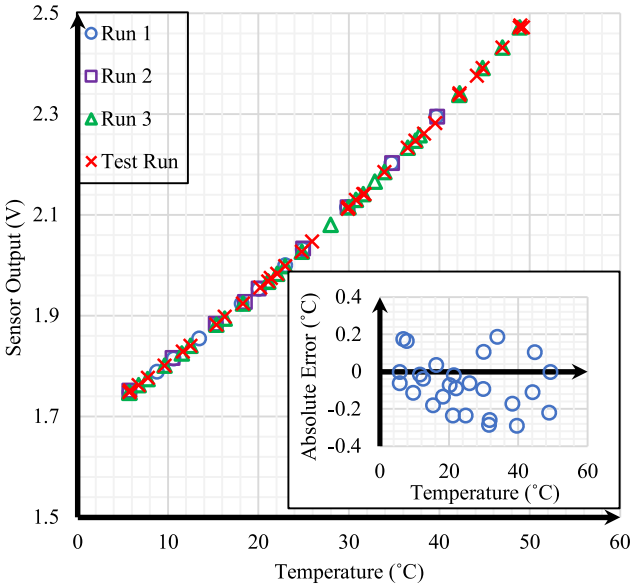

Fig. 13. Performance of the temperature sensor.

was varied from 5 to 50°C (see Fig. 13), and a correlation was established (2) between sensor output and reference temperature

$$T = -18.8251 \cdot V_t^2 + 138.4403 \cdot V_t - 178.6271 \tag{2}$$

where T denotes temperature (°C) and V_t denotes voltage output (V) of temperature sensor. Equation (2) was applied to predict temperatures of the test run and the results are shown inset in Fig. 13. The absolute errors of (2) range from -0.29 to 0.19 °C.

The assessment of the conductivity sensor was performed using sodium chloride solutions with different concentrations. Sensor outputs were then compared with the readings from a HI-98304 pocket conductivity meter. The resolution and the accuracy of the reference meter are 0.01 mS/cm and 2% F.S., respectively. Two sets of tests were carried out with different

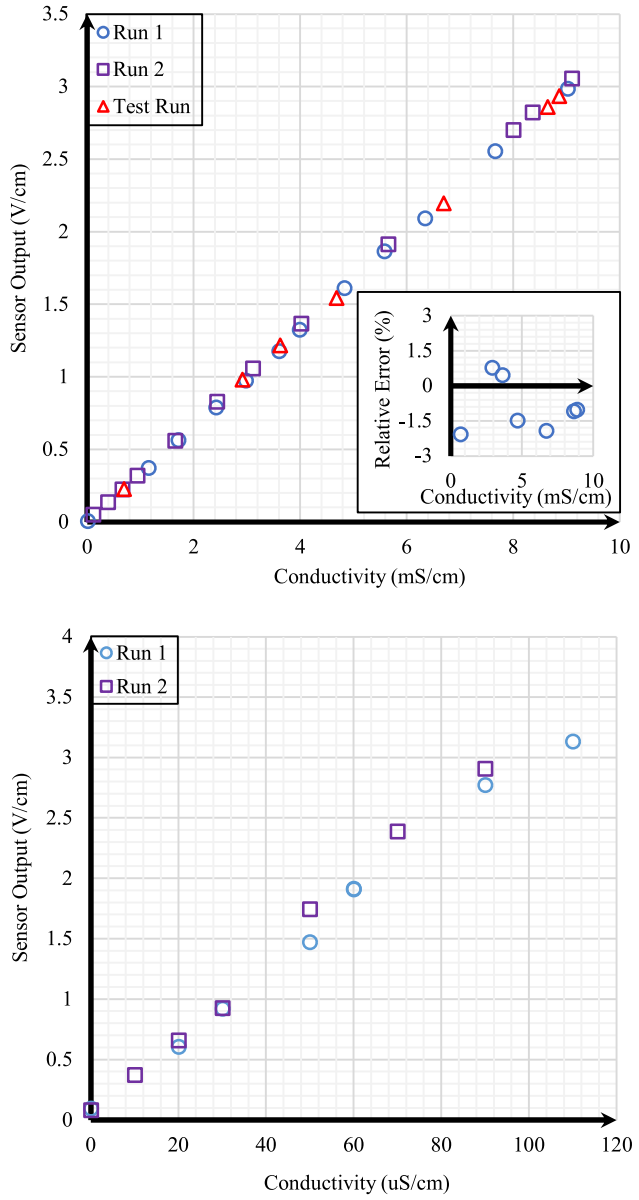

Fig. 14. Performance of the conductivity sensor. Upper: 0–10 mS/cm. Lower: 0–100 mS/cm.

conductivity ranges: 0 to 100μS/cm and 0 to 10 mS/cm, by switching the gain of the inverting amplifier in the readout circuit. According to the data in Fig. 13, the following fitting equation was established for the conductivity sensor:

$$C = 2.9888 \cdot V_c + 0.0023. \tag{3}$$

Here, C denotes conductivity (mS/cm) and V_c denotes the voltage output (V) of the conductivity sensor. Fig. 13 shows the accuracy of (3) in predicting conductivities. The relative errors range from -2.06% to 0.77%. Another test was done for the conductivity sensor with a lower measurement range of 0–100 μS/cm by switching the gain of the inverting amplifier in the readout circuit, and the results are shown in Fig. 14.

Flow sensor testing was performed in both the 1-inch and 2-inch test sections of the flow rig. The water flow was set between 20 L/min and 80 L/min by the pump controller. As the reference meter was installed in the 1-inch test section, the pump motor speed was adopted as reference of the tests on the 2-inch section. The test results are plotted in Fig. 15 and the following correlations were established by data fitting:

$$1-\text{inch test: } Q = 1.0425 \cdot \sqrt{\Delta P} + 2.0128$$
$$2-\text{inch test: } \omega = 0.1664 \cdot \sqrt{\Delta P} + 0.2372.$$

Here, Q denotes water flow rate (L/min), ΔP is the differential pressure (Pa), and ω is the motor speed (krpm). To assess these equations, another two sets of experiment were conducted and the relative errors of (4) and (5) were from -3.00% to 4.70%, and -5.05% to 3.43%, respectively.

It is noted that the sensing translation (1)–(4) are presented here with full parametric accuracy (i.e., number of significant digits), for consistency with the reported accuracy values. These calibration values are programmable and can be adjusted by calibration during installation or dynamically during operation in a self-calibration scheme, if adequate feedback references are provided.

For data transmission using BLE, a laptop was used as the central BLE device. A LabVIEW user interface together with a USB BLE dongle was used to visualize sensor data; the same set-up could potentially allow more user control for sensor sampling rates, battery information, etc. Acquired sensor results are available in a Git repository [28]. The nRF52840 – SARA-N2 interface functionally was confirmed by AT command communication tests. The NB-IoT connectivity was not demonstrated as the corresponding network level service is currently only offered in pilot laboratories operating in certain regions, such as the Vodafone OpenLab in Newbury, U.K. [29].

VII. Opportunities

The multisensor architecture introduced in this article includes a simple and effective electronic design, adequate sensing accuracy and repeatability, and a multistage parametric duty-cycling protocol for power consumption minimization. It also includes a modular and expandable design, with interchangeable sensing probes, adaptation to different pipeline diameters and a methodical, hot-tapping installation method. It integrates external environment sensors that can provide complementary data and expand the sensing services range. Finally, the system demonstrates adequate sealing and state-of-the-art Industrial Internet-of-Things connectivity.

These features are validated experimentally, and they offer a complete sensor node deployment solution. The introduction of small scale hot-tapping for sensing in particular, in combination with the modular architecture, offers a minimal required installation and configuration expertise, minimal disruption, retrofitting capability of a high-end sensing solution. The installation solution offered is demonstrated in integration with sensing and connectivity operation. It opens the way forward for development and testing of a range of highly desirable water monitoring features and capabilities, some of which are summarized in the remainder of this Section.

Leakage detection continues to be a central priority of WSNs in the water supply chain, mainly due to the extended

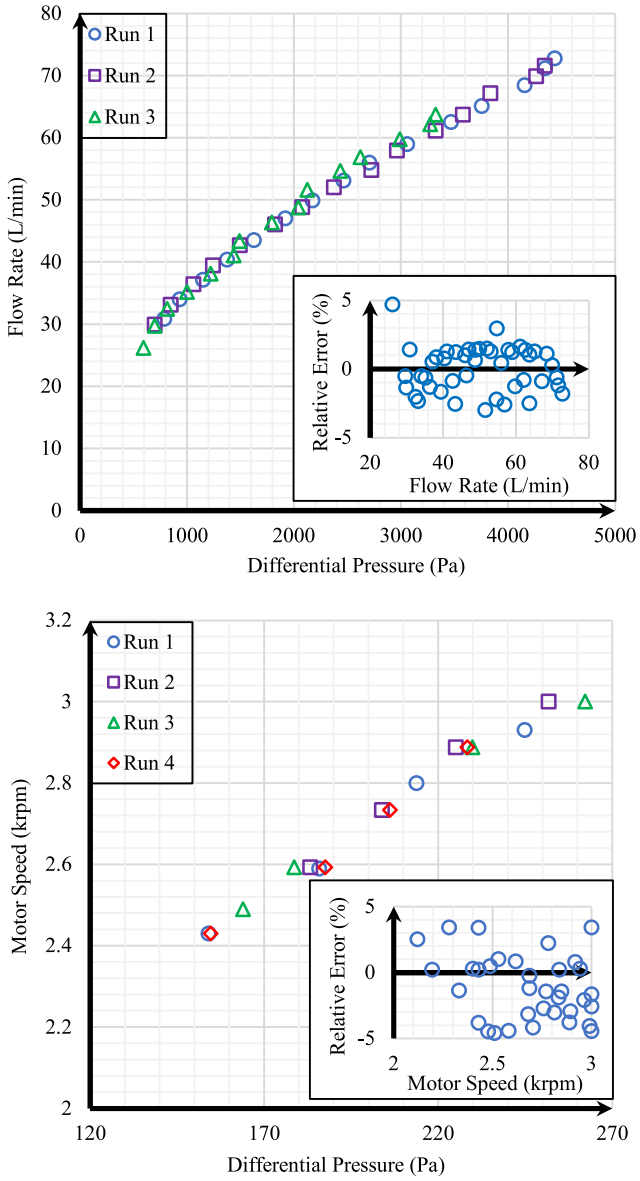

Fig. 15. Performance of flow sensor. Upper: 1-inch test section. Lower: 2-inch test section.

scale at which it occurs [30]. Apart from its economic impact, it is often discussed as a priority for preserving water as a valuable commodity and to ensure sustainable use for the near and long term future, but also for regions with limited water access [3]. On the other hand, monitoring and control of quality is very diverse and includes chemical analysis as well as the detection of events and operational parameters that affect quality, such as turbidity, flow, and backflow [2], [31]–[44]. It also includes reservoir stations, such as stormwater retentions ponds [45]. In the particular case of contamination, early and localized detection [46], [47] is critical to safety, and therefore, the density of sensors, along with installation topology strategy, is decisive for the effective application of data analysis and detection algorithms and subsequently for control, alarming, infiltration and various response methods [48].

The sensor architecture introduced in this article is applicable to both leakage and quality monitoring through its modular, minimally invasive multisensor node approach. Additional sensors, such as pH, turbidity, and particle concentration meters can be added straightforwardly, as corresponding commercial components suit the probe immersion approach and fit onto the Ø 6 mm probe size used.

The density of sensor deployment required in a water network is key to achieving a sufficient monitoring service at reasonable cost. It is a very important parameter and is closely related to the value and use of monitoring data at network level. The water network topology in combination with general rules and exceptions about locations and moments of special interest is required to identify a suitable number of sensors. This information is not readily available and in practice is very difficult to know in advance. Therefore, a gradual deployment strategy may often be preferable, in which a sparse initial grid is installed initially, and points of interests for more detailed sensing are subsequently identified. In this direction, the minimally invasive and portable architecture proposed in this article offers the possibility of selectable, configurable, multistage or dynamic deployment and activation.

Apart from the aforementioned direct water leakage and quality benefits, another important case of interest for water monitoring, which is also linked to its increasing value as a commodity for demographic and climate change reasons, is its monitoring for blocking potential security threats, including malicious attacks by deliberate water network contamination. Such a threat has been determined as one of the most difficult to address. Therefore, the installation of an effective water contamination monitoring system is of strategic importance both for counteracting malicious events as well as for discouraging threats and increasing the sense of safety and security among the global population. Again, adequate sensor density and optimized topology are critical for the efficiency of such monitoring systems. In [49], a comparison of different WSN solutions, coined the battle of the water sensor networks, was presented, employing common figures of merit for the efficiency of 15 different WSN approaches.

The security of sensors and sensing data is in turn also critical. Data integrity and protection from tampering and theft can be enhanced by sensor location tracking and software activity logging. Including authenticated security logs in data package network traffic could offer a measurable level of confidence for the validity and protection of gathered data. Hardware implemented location tracking and authentication could offer a significant advantage for infrastructure sensor deployment in this direction, especially for sensitive data applications [50]–[52].

Finally, infrastructure surveillance also benefits from the deployment of WSNs, including availability, utility, optimization of operations, and real-time meters at reservoirs, distribution points and consumer locations. Potential advantages that have been identified include measurement accuracy, fault and theft detection, remote control, exploitation of real-time data for efficient and environmentally friendly consumption, usage balancing, and enforcement of restrictions during drought periods. The introduced sensor node architecture offers the necessary data to the network for further analysis and exploitation.

This article describes the performance and measurements available for a single multisensor node. The expected benefits to an operator are at the higher system level in terms of insights and actionable information related to the specific challenges faced (productivity, water quality, network performance, pipe burst, etc). The normal approach to instrumenting a network will depend on the WSNs specific requirements and areas of focus. Today's instruments typically measure a single measurand; therefore the operator will rarely be able to instrument a system to an ideal or desired level. The multisensor design presented here can be configured with specific measurands relevant to the challenges faced by a WSN and in many cases retrofitted. Using wireless communication, the data from an array of multisensor nodes and existing instruments can be aggregated and data analytics applied to deliver a system level overview with specific insights into a particular challenge. A shift toward overall sensing solutions which consider the process at a macrolevel can deliver targeted benefits to operators.

VIII. Conclusion

Water sensor networks can improve usage efficiency by leakage reduction, quality assurance and operations optimization, with important economic, life quality and environmental benefits. As the sensor node and network technologies have progressed rapidly and reached adequate maturity in the last decade, integration and installation methods are becoming key elements to their adoption by the infrastructure industry. This is especially important for water quality sensors, which typically require immersion. In addition, a quantified estimation of sensing cost and benefit is often not straightforward, and important questions on required data scale, topography and frequency as well as on data exploitation and value are pending.

In this article, an integrated multisensor architecture for water infrastructure monitoring is presented. A minimally invasive hot-tapping installation method is introduced that offers a practical, cost-effective and scalable option for immersion sensors. A modular design approach allows interchangeable, serviceable, and upgradeable multisensor probes to be developed and used. A prototype offering water pipeline pressure, temperature, flow and conductivity sensing, as well as complementary external environmental sensing of pressure, temperature, and vibration, is presented, in integration with internal storage, processing and wireless communication capabilities, including BLE and NB-IoT. Operation at adequate sensing resolution is demonstrated, including static pressure tests which also demonstrate a successful sealed installation for pressures over 8.5 bar.

An overview of opportunities arising from the proposed multisensor architecture and installation method reveals that a scalable, multistage deployment approach may be beneficial in terms of reduced initial investment cost, identification of locations and measurands of priority interest, quantification of sensing benefit, and a gradual development according to requirements and limitations of water infrastructure. Priorities identified by potential technology users include leakage detection, quality, security and threat management, data transparency and operational optimization.

Overall, the system level demonstration of a minimally invasive, modular, multisensor has been presented, comprising state-of-the-art sensing, processing and networking subsystems, which contributes a key and likely pivotal missing element toward the implementation of leakage and quality sensor networks.

References

[1] M. S. BenSaleh, S. M. Qasim, A. M. Obeid, and A. Garcia-Ortiz, "A review on wireless sensor network for water pipeline monitoring applications," in *Proc. Int. Conf. Collaboration Technol. Syst.*, 2013, pp. 128–131.

[2] H. B. Glasgow, J. M. Burkholder, R. E. Reed, A. J. Lewitus, and J. E. Kleinman, "Real-time remote monitoring of water quality: A review of current applications, and advancements in sensor, telemetry, and computing technologies," *J. Exp. Mar. Biol. Ecol.*, vol. 300, nos. 1–2, pp. 409–448, Mar. 2004.

[3] A. M. Obeid, F. Karray, M. W. Jmal, M. Abid, S. M. Qasim, and M. S. BenSaleh, "Towards realisation of wireless sensor network-based water pipeline monitoring systems: A comprehensive review of techniques and platforms," *IET Sci. Meas. Tech.*, vol. 10, no. 5, pp. 420–426, Aug. 2016.

[4] E. Katsiri and C. Makropoulos, "An ontology framework for decentralized water management and analytics using wireless sensor networks," *Desalination Water Treatment*, vol. 57, no. 54, pp. 26355–26368, Nov. 2016.

[5] A. U. Alam, D. Clyne, H. Jin, N.-X. Hu, and M. J. Deen, "Fully Integrated, simple, and low-cost electrochemical sensor array for in situ water quality monitoring," *ACS Sens.*, vol. 5, no. 2, pp. 412–422, 2020.

[6] Y. Qin *et al.*, "Integrated water quality monitoring system with pH, free chlorine, and temperature sensors," *Sens. Actuators B, Chem.*, vol. 255, pp. 781–790, Feb. 2018.

[7] Y. Xie, Z. Wen, Z. Mo, Z. Yu, and K. Wei, "Implementation of an automatic and miniature on-line multi-parameter water quality monitoring system and experimental determination of chemical oxygen demand and ammonia-nitrogen," *Water Sci. Technol.*, vol. 73, no. 3, pp. 697–706, 2016.

[8] Kamstrup. (2020). *Smart Water Meters & Devices*. [Online]. Available: www.kamstrup.com/en-en/water-solutions/smart-water-meters

[9] SweetSense. (2020). *Fixing the Internet of Broken Things*. [Online]. Available: www.sweetsensors.com/our-technology/

[10] Sensus. (2020). *640C/640MC Water Meter*. [Online]. Available: sensus.com/products/640c-640mc-water-meter/

[11] M. E. Kiziroglou, D. E. Boyle, S. W. Wright, and E. M. Yeatman, "Acoustic power delivery to pipeline monitoring wireless sensors," *Ultrasonics*, vol. 77, pp. 54–60, May 2017.

[12] Katronic. (2020). *Safeguarding Potable Water Supply Under Busy Airport Runway*. [Online]. Available: www.katronic.com

[13] MeritSensor. (2020). *Merit Sensor HM Series*. [Online]. Available: meritsensor.com/products/hm-series/

[14] Arian. (2020). *Theory Overview of Flow Measurement Using Differential Pressure Devices Based on ISO-5167 Standard*. [Online]. Available: www.arian.cl/ingles/support.htm

[15] AMS. (Nov. 2019). *AMS 5915: Amplified Pressure Sensor with Digital Output (I) (Rev. 3.1 ed.)* [Online]. Available: www.amsys-sensor.com/products/pressure-sensor/ams5915-digital-pressure-sensor-5mbar-to-10-bar/

[16] IST-AG. (2020). *LFS1305 Conductivity Sensor For Various Conductivity Measurement Applications (DCLFS1305_E2.3.0 ed.)* [Online]. Available: www.ist-ag.com/en/products-services/conductivity-sensors

[17] Maxim. (2020). *High-Efficiency, Low-Supply-Current, Compact, Step-Up DC-DC Converters, MAX1674/MAX1675/MAX1676 (19–1360; Rev 3; 3/00)*. [Online]. Available: www.maximintegrated.com/en/products/power/switching-regulators/MAX1674.html

[18] Nordic. (2019). *Product Specification*. [Online]. Available: nRF52840 infocenter.nordicsemi.com/index.jsp?topic=%2Fps_nrf52840%2Fkeyfeatures_html5.html

[19] Ublox. (2020). *Power-Optimized NB-IoT (LTE Cat NB1) Modules, SARA-N2 Series (UBX-15025564: R18)*. [Online]. Available: www.u-blox.com/en/product/sara-n2-series

[20] SiliconLabs. (2020). *I2C Humidity And Temperature Sensor, Si7021–A20 (Rev. 1.2 8/16 ed.)* [Online]. Available: www.silabs.com/sensors/humidity/si7006-13-20-21-34/device.si7021-a20-gm

[21] STMicroelectronics. (2016). *MEMS Digital Output Motion Sensor: Ultra-Low-Power High-Performance 3-Axis 'Nano' Accelerometer (DocID17530 Rev 2 ed.)* [Online]. Available: www.st.com/en/mems-and-sensors/lis3dh.html

[22] S. Tatham. (2020). *PuTTY: A Free SSH and Telnet Client*. [Online]. Available: www.chiark.greenend.org.uk/∼sgtatham/putty/

[23] M. Collotta, G. Pau, T. Talty, and O. K. Tonguz, "Bluetooth 5: A concrete step forward toward the IoT," *IEEE Commun. Mag.*, vol. 56, no. 7, pp. 125–131, Jul. 2018.

[24] L. Feltrin *et al.*, "Narrowband IoT: A survey on downlink and uplink perspectives," *IEEE Wireless Commun.*, vol. 26, no. 1, pp. 78–86, Feb. 2019.

[25] L. Chettri and R. Bera, "A comprehensive survey on Internet of Things (IoT) toward 5G wireless systems," *IEEE Internet Things J.*, vol. 7, no. 1, pp. 16–32, Jan. 2020.

[26] Jauch. (2018). *Jauch Battery Solutions, LP735977JH*. [Online]. Available: www.jauch.com/en-INT/products/battery_technology/getPrm/batteries/LithiumPolymerBatteries/

[27] *Measurement of Fluid Flow by Means of Pressure Differential Devices Inserted in Circular Cross-Section Conduits Running Full—Part 1: General Principles and Requirements, International Organization of Standardization*, ISO Standard 5167-1, 2003.

[28] S. K. E. Yang. (2020). *Imperial College London Git Repository for ABB Research on Water Sensing*. [Online]. Available: github.com/skeyang/MkIV-sensor-data.git

[29] Vodafone. (2020). *Specialized Narrow-Band IoT Services*. [Online]. Available: www.vodafone.com/business/iot/managed-iot-connectivity/nb-iot#narrowbandiot-applications-and-solutions

[30] M. I. M. Ismail *et al.*, "A review of vibration detection methods using accelerometer sensors for water pipeline leakage," *IEEE Access*, vol. 7, pp. 51965–51981, 2019.

[31] O. S. Adedoja, Y. Hamam, B. Khalaf, and R. Sadiku, "A state-of-the-art review of an optimal sensor placement for contaminant warning system in a water distribution network," *Urban Water J.*, vol. 15, no. 10, pp. 985–1000, Nov. 2018.

[32] S. Archer, "A review of sensors for remote continuous automatic monitoring of water-quality," *Chem. Ind.*, vol. 15, no. 15, pp. 613–617, 1980. [Online]. Available: https://apps.webofknowledge.com/full_record.do?product=WOS&search_mode=GeneralSearch&qid=1&SID=E2sWOhxMIkPv4ySxX8Z&page=1&doc=5

[33] J. Bhardwaj, K. K. Gupta, and R. Gupta, "A review of emerging trends on water quality measurement sensors," presented at the Int. Conf. Technol. Sustain. Develop., 2015.

[34] J. B. Chang, G. H. Zhou, E. R. Christensen, R. Heideman, and J. H. Chen, "Graphene-based sensors for detection of heavy metals in water: A review," *Anal. Bioanal. Chem.*, vol. 406, no. 16, pp. 3957–3975, Jun. 2014.

[35] W. E. Hart and R. Murray, "Review of sensor placement strategies for contamination warning systems in drinking water distribution systems," *J. Water Resour. Plann. Manag.*, vol. 136, no. 6, pp. 611–619, Nov./Dec. 2010.

[36] P. Kruse, "Review on water quality sensors," *J. Phys. D, Appl. Phys.*, vol. 51, no. 20, May 2018, Art. no. 203002.

[37] F. Q. Li, Z. G. Yu, X. D. Han, and R. Y. Lai, "Electrochemical aptamer-based sensors for food and water analysis: A review," *Analytica Chimica Acta*, vol. 1051, pp. 1–23, Mar. 2019.

[38] J. Macpherson, "In the lab development of carbon based electrochemical sensors for water analysis: Johnson Matthey Technology Review features new laboratory research," *Johnson Matthey Technol. Rev.*, vol. 59, no. 1, pp. 52–55, Jan. 2015.

[39] S. O. Olatinwo and T. H. Joubert, "Energy efficient solutions in wireless sensor systems for water quality monitoring: A review," *IEEE Sensors J.*, vol. 19, no. 5, pp. 1596–1625, Mar. 2019.

[40] L. R. Pokhrel *et al.*, "Novel carbon nanotube (CNT)-based ultrasensitive sensors for trace mercury(II) detection in water: A review," *Sci. Total Environ.*, vol. 574, pp. 1379–1388, Jan. 2017.

[41] S. R. J. Ramson, D. Bhavanam, S. Draksharam, A. Kumar, D. J. Moni, and D. J. Moni, "Sensor networks based water quality monitoring systems for intensive fish culture: A review," presented at the 4th Int. Conf. Devices Circuits Syst., 2018.

[42] S. Rathi, R. Gupta, and L. Ormsbee, "A review of sensor placement objective metrics for contamination detection in water distribution networks," *Water Sci. Technol. Water Supply*, vol. 15, no. 5, pp. 898–917, 2015.

[43] C. Wang and C. X. Yu, "Detection of chemical pollutants in water using gold nanoparticles as sensors: A review," *Rev. Anal. Chem.*, vol. 32, no. 1, pp. 1–14, Feb. 2013.

[44] J. F. Zhang and S. L. Li, "Sensors for detection of Cr(VI) in water: A review," *Int. J. Environ. Anal. Chem.*, to be published.

[45] Q. Qian, B. Sun, X. C. Li, F. Sun, C. J. Lin, and L. P. Jiang, "Water quality evaluation on an urban stormwater retention pond using wireless sensor networks and hydrodynamic modeling," *J. Irrig. Drain. Eng.*, vol. 145, no. 12, Dec. 2019, Art. no. 05019011.

[46] T. P. Lambrou, C. G. Panayiotou, and M. M. Polycarpou, "Contamination detection in drinking water distribution systems using sensor networks," in *Proc. Eur. Control Conf.*, 2015, pp. 3298–3303.

[47] J. Yang and X. Luo, "A study on water pollution source localization in sensor networks," *J. Sensors*, vol. 2016, no. 3, 2016, Art. no. 9528050.

[48] M. Comboul and R. Ghanem, "Value of information in the design of resilient water distribution sensor networks," *J. Water Resour. Plann. Manag.*, vol. 139, no. 4, pp. 449–455, Jul. 2013.

[49] A. Ostfeld, J. G. Uber, E. Salomons, and J. W. Berry, "The battle of the water sensor networks (BWSN): A design challenge for engineers and algorithms," *J. Water Resour. Plann. Manag.*, vol. 134, no. 6, pp. 556–568, Nov./Dec. 2008.

[50] Y.-J. Huang, C.-C. Yuan, M.-K. Chen, W.-C. Lin, and H.-C. Teng, "Hardware implementation of RFID mutual authentication protocol," *IEEE Trans. Ind. Electron.*, vol. 57, no. 5, pp. 1573–1582, May 2010.

[51] J. Ni, K. Zhang, and A. V. Vasilakos, "Security and privacy for mobile edge caching: Challenges and solutions," *IEEE Wireless Commun.*, early access, Dec. 21, 2020, doi: 10.1109/MWC.001.2000329.

[52] I. Mistry, S. Tanwar, S. Tyagi, and N. Kumar, "Blockchain for 5G-enabled IoT for industrial automation: A systematic review, solutions, and challenges," *Mech. Syst. Signal Process.*, vol. 135, Jan. 2020, Art. no. 106382.